Available online at www.sciencedirect.com
ScienceDirect
Journal of Nuclear Materials 375 (2008) 120–134
journal of nuclear materials
www.elsevier.com/locate/jnucmat

Molecular dynamics study of acoustic velocity in silicate glass under irradiation

N. Deladerriere [a], J.M. Delaye [a,*], F. Augereau [b], G. Despaux [b], S. Peuget [c]

[a] CEA Marcoule, DEN/SECM/LCLT, BP17171, 30207 Bagnols-sur-Cèze, France
[b] Université de Montpellier II, LAIN, Place Eugène Bataillon, 34095 Montpellier, France
[c] CEA Marcoule, DEN/SECM/LMPA, BP17171, 30207 Bagnols-sur-Cèze, France

Received 8 October 2007; accepted 21 November 2007

Abstract

The development of a molecular dynamics method simulating the propagation of acoustic waves allowed their propagation velocities to be measured in borosilicate glasses. The qualitative results obtained in glass irradiated by heavy ions correctly reproduces the experimental results, i.e. a reduction in the acoustic wave propagation velocity in irradiated glass. These changes in the mechanical properties were correlated with structural changes, in particular increased disorder in the glass. The greater disorder results in broadening of the characteristic distributions of the glass: distances, angles, and ring sizes. Similarities were clearly observed between the effects of irradiation and the effects of higher quenching rates on the acoustic wave propagation velocities. An additional study of glass artificially expanded by homothetic volume transformation shows that a reduction in acoustic velocity is not necessarily associated with swelling. The artificial volume change combined with increased stresses in the glass results in higher acoustic velocities.

PACS: 62.20.−x; 71.15.Pd; 78.55.Qr

1. Introduction

Nuclear glass used for radioactive waste containment is subjected to the effects of alpha, beta and gamma decay [1]. Beta–gamma decay produces electronic excitation whereas alpha decay produces not only electronic excitation with an energy of about 4 MeV due to the α particle but also the emission of a recoil nucleus at an energy between 70 keV and 100 keV.

Previous studies have shown that ballistic collisions due to the propagation of the recoil nucleus are the main cause of variations in the hardness [2,3] and density [4] of nuclear glass. Measurements on a curium-doped complex nuclear glass reveal a hardness reduction of about 30% as the alpha decay dose increases. The density also diminishes and appears to stabilize after an alpha decay dose of 2×10^{18} α/g.

The ballistic effects arising from the alpha disintegration recoil nucleus can be modeled by classical molecular dynamics. This approach disregards the effects of electronic losses. The increased computing power available today recently allowed us to simulate series of displacement cascades generated by recoil nuclei in a simulation cell containing several tens of thousands of atoms [5,6]. Each cascade was simulated in three steps:

- acceleration of a heavy ion and simulation of the cascade of ballistic collisions; the volume was maintained constant during this step;
- relaxation in the isothermal isobaric system [7] to determine the new equilibrium volume of the irradiated cell;
- relaxation of the structure at constant volume (as determined during the preceding step) before the following cascade.

* Corresponding author. Tel.: +33 466791794; fax: +33 466797708.
E-mail addresses: jean-marc.delaye@cea.fr, j.-m.delaye@cea.fr (J.M. Delaye).

0022-3115/$ - see front matter © 2007 Published by Elsevier B.V.
doi:10.1016/j.jnucmat.2007.11.002

This method allowed us to monitor atomic-scale variations in the structure as well as volume changes during the series of displacement cascades at 4 keV.

The French 'R7T7' nuclear glass [8] used for containment of radioactive materials comprises some thirty oxides and cannot currently be modeled by molecular dynamics. Simulations are therefore based on simplified glass models subjected to an accumulation of 4 keV cascades. These energies are far from the actual energy levels, as the limitations of existing computers prevent simulating realistic recoil nuclei doses of 70 keV or 100 keV within a reasonable time frame. The glass models are nevertheless representative of R7T7 glass because they conserve the molar ratios among species and simulate the mixture of network formers and network modifiers. Recent experiments have shown analogies between the behavior of simple glasses and R7T7 glass under irradiation [9].

Most of the results described in this article were obtained with a ternary glass known as CJ1, comprising 65.56 wt% SiO_2, 14.21 wt% Na_2O and 20.23 wt% B_2O_3 [10].

We focused on the difference in the propagation velocity of acoustic waves between pristine and irradiated glass. A novel method based on classical molecular dynamics was implemented for this purpose. The method, based on the experimental procedure, consisted in initiating a displacement wave in the glass structure and measuring its propagation velocity. Periodic square-wave pulses were applied to a segment of atoms at one end of the simulation cell and their propagation was quantified in the glass structure. Trial and error tests were necessary to optimize the pulse amplitude and duration.

Acoustic waves were simulated in the NVE ensemble (constant atom number, volume and energy) in cubic cells with a volume of approximately 900 nm^3 (different cells of comparable volumes were used).

Knowing the acoustic propagation velocity it is possible to determine the elastic moduli from the relations between the elastic moduli and the longitudinal and transverse propagation velocities

$$E = \rho \frac{V_T^2\left(3V_L^2 - 4V_T^2\right)}{V_L^2 - V_T^2}. \tag{1}$$

In Eq. (1), V_L and V_T are the longitudinal and transverse velocities, and E is Young's modulus.

Acoustic microscopy [11] is capable of measuring the Rayleigh velocity, V_R, which is expressed in terms of V_L and V_T in

$$V_R = V_T \frac{0.715 - 0.995\left(\frac{V_T}{V_L}\right)^2}{0.75 - \left(\frac{V_T}{V_L}\right)^2}. \tag{2}$$

Experiments in which glass specimens were externally irradiated by multi-energy ions revealed changes in their mechanical properties, and more precisely a reduction in the longitudinal and transverse propagation velocities [12] (paragraph III. A. in this paper) and, from Eq. (1), a reduction in Young's modulus. These experimental results were corroborated by longitudinal and transverse acoustic velocity measurements obtained by classical molecular dynamics.

By reproducing the experimental phenomena we were able to correlate macroscopic variations and structural changes at atomic scale, and thus propose explanation for the diminishing propagation velocities of acoustic waves under irradiation.

2. Methodology

2.1. Modeling glass structure and displacement cascades

Classical molecular dynamics simulations of glass structure and displacement cascades are performed in the microcanonical (NVE) ensemble [5,13,14]. Born–Mayer–Huggins interaction potentials represent ionic and covalent interactions as a sum of pair terms ϕ_2 and three-body terms ϕ_3. The analytical form of the pair potentials is the following:

$$\phi_2(r_{ij}) = A\exp\left(-\frac{r_{ij}}{\rho}\right) + \frac{q_i q_j}{r_{ij}}\operatorname{erfc}(\alpha r_{ij}), \tag{3}$$

where $r_{ij(ik)}$ is the distance between atoms i and j (i and k); q_i and q_j are the charges of atoms i and j; A and ρ are adjustable parameters dependent on the atomic species considered.

Integer charges are used to represent interactions between ions (Si^{4+}, B^{3+}, Na^{+}, O^{2-}). The erfc term corresponds to the real component of the Ewald sum [15] for modeling screened Coulomb interactions. The Ewald sum component in reciprocal space is disregarded to limit the computation time. The parameter value is 0.263 $Å^{-1}$ and cutoff radii of 8 Å and 10 Å are used for the exponential term and erfc term, respectively.

$$\phi_3(r_{ij}, r_{ik}, \theta_{jik}) = \lambda\exp\left(\frac{\gamma}{r_{ij} - r_c} + \frac{\gamma}{r_{ik} - r_c}\right) \times \left(\cos\theta_{jik} - \cos\theta_0\right)^2, \tag{4}$$

where θ_{jik} is the angle formed by the jik atom triplet; λ and γ are adjustable parameters dependent on the chemical nature of the atom considered. The three-body terms are based on work by Stillinger et al. [16], and these parameters were fitted to silicate glasses by Feuston et al. [17].

Short-range interactions are processed using Ziegler–Biersack–Littmark (ZBL) potentials [18]. Short-range interactions appear when simulating cascades of ballistic collisions.

The potential parameters are detailed in Ref. [5]. The time steps are also progressively fit according to the maximum instantaneous atomic velocity [19].

The simulated glasses consist of 64 000 atoms in a cubic cell with an initial edge dimension of 96.894 Å; the volume changes from one cascade to the next. The CJ1 glass composition is used. Conventional periodic conditions are used to repeat the simulation cell in three dimensions.

2.2. Acoustic velocity measurement methodology

The simulation methodology used to measure the acoustic velocity consists in initiating a displacement wave and measuring the wave propagation time in the glass structure.

The simulation cell is broken down into 'slabs' (Fig. 1) at right angles to the wave propagation direction. The slabs are 3 Å thick, and the simulation cell includes 33 or 34 slabs numbered from 1 (depending on the cell volume), each containing about 1900 atoms.

The atoms belonging to the extreme left-hand slab (shown in black in Fig. 1) are displaced along the x-axis in the case of a longitudinal wave and at right angles (y,z) in the case of a transverse wave. The initial displacement is induced by a pulse with an amplitude of 0.2 Å. To avoid transmitting the acoustic wave through the opposite face, which would create resonance in the simulation cell, the atoms belonging to the slabs at the opposite end (light gray in Fig. 1) are frozen. The number of frozen slabs is calculated so the thickness is not less than the cutoff radius used for the interaction potentials (i.e. 10 Å).

The displacement applied to the initial slab consists of positive then negative pulses along the x-axis. The wave train visible in Fig. 2 comprises a 1 ps pulse duration, with 5 ps between pulses. The propagation time analysis is based on the center-of-mass positions of the mobile slabs. The atoms in each slab are initially identified and do not change during the simulation. The slab center-of-mass coordinates are calculated at each time step, as are the mean position coordinates of the atoms identified in the slab. The difference between instantaneous center of mass and its initial position indicates the slab displacement. Typical displacements are shown in Fig. 3(a). The successive center-of-mass positions for the initial slab (bold line) and for three mobile slabs (thin lines) are shown.

A method was developed to measure the propagation velocity from the derivatives of the signals (computed during the simulation) according to a finite differences equation

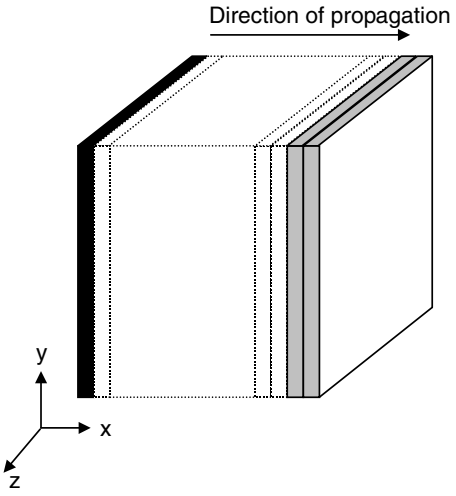

Fig. 1. Schematic view of simulation cell.

$$\frac{\mathrm{d}x}{\mathrm{d}t} = \frac{x_{i+1} - x_{i-1}}{2\Delta t}, \tag{5}$$

where x_{i+1} and x_{i-1} are the center-of-mass positions at time values t_{i+1} and t_{i-1}; Δt is the computation time step, i.e. 1 fs. The resulting curve for the derivative is shown in Fig. 3(b) with the same time scale as for the center-of-mass displacement curves (Fig. 3(a)). Each derivative has a maximum for the pulse leading edge and a minimum for the trailing edge.

The time shift, which is directly proportional to the wave propagation velocity, is measured by calculating the differences between the maxima of the derivatives (visible in the enlarged inset of Fig. 3(b)) with the maximum of the derivative of the first mobile slab (slab number 2) as the time reference point.

To limit the perturbations due to the thermal agitation movement of the atoms, the simulations are performed at a temperature of 10 K; the temperature is maintained constant by regularly rescaling the atomic velocities. A conditional temperature control is implemented to avoid superimposing the velocity rescaling on the dynamics corresponding to the passage of the acoustic wave: the temperature is unrestricted during the acoustic wave propagation time inside the cell, then the temperature is controlled before the passage of the next pulse. The temperature control phases thus alternate with the square-wave propagation phases.

The temperature profile during the calculation is shown in Fig. 2. Each pulse train corresponds to a temperature jump. The two successive temperature increases are due to the energy supplied during the initial atom displacement (in one direction, then the other). Controlling the atomic velocity allows the temperature to drop to 10 K before the next pulse.

The propagation velocity is calculated in each slab from the extreme positions of the center-of-mass displacement derivative. The velocity is plotted versus the slab number in Fig. 4.

Three successive velocity regimes are visible within the simulation cell:

- an initial regime of high velocities near the first slab,
- a regime of virtually constant velocities,
- a 'disturbed' regime.

The third regime is disturbed mainly by the acoustic wave rebounding off the frozen slabs at the far end of the cell that prevent the wave from being transmitted from one surface to the another. Accurate measurements are difficult to obtain in the first regime due to the very thin slabs.

The final measurement is therefore performed on the intermediate slabs at virtually constant velocity. The number of slabs taken into account to calculate the mean propagation velocity is variable, depending on the shape of the resulting velocity profile. Except for the values measured in the disturbed zone the profile exhibits satisfactory pulse repeatability as shown in Fig. 4.

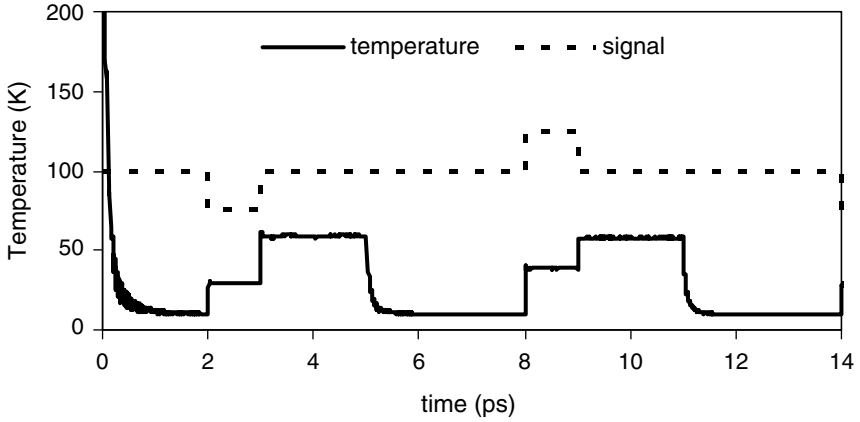

Fig. 2. System temperature (in black) and initial displacement of slab 1 (in grey) versus time. The atomic displacement curve is indicated for reference only, to account for the temperature jumps.

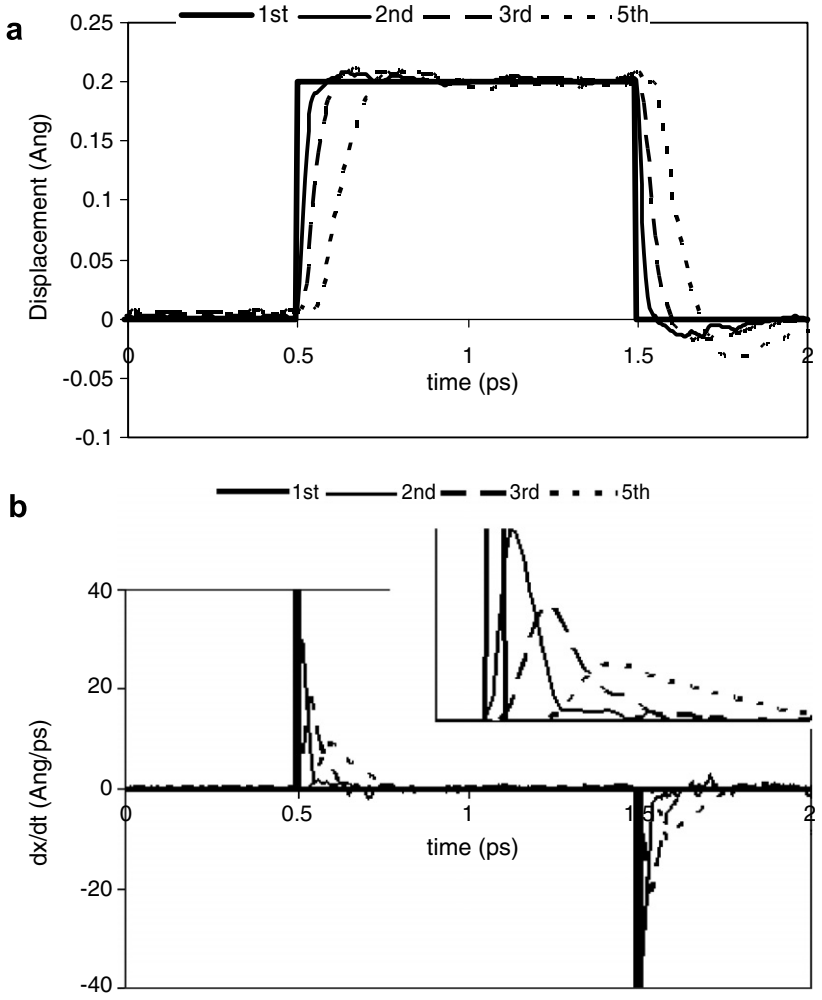

Fig. 3. Slab center-of-mass displacements versus time (a) and corresponding derivatives (b).

2.3. Artificial density variation

Glass structures were also prepared with different densities starting from an unirradiated glass. Instantaneous swelling or compression was applied to the structures by homothetic transformation of all the atom positions. Following the volume change, no temperature control is exerted on the system for 10 000 time steps. The temperature thus increases according to the reorganization of the glass structure. After 10 000 time steps, the system is cooled to 293 K by regularly rescaling the atomic velocities during the subsequent 10 000 steps. As the objective is to obtain a

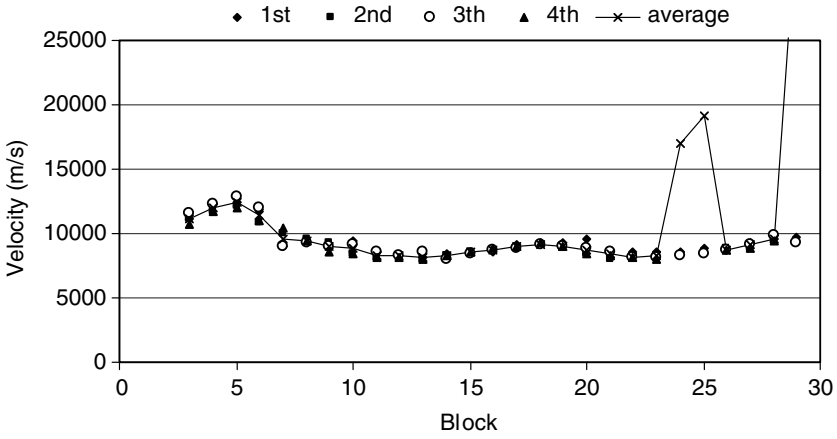

Fig. 4. Velocities measured in successive slabs for different pulses.

structure as close as possible to the initial structure but with a different volume, no relaxation is performed. This results in a nonzero pressure in the glass: positive for compression and negative for expansion (Fig. 5).

A second version of these structures with annealing and quenching at 10^{14} K/s was prepared to relieve the stresses arising from the volume change. In this case, quenching was simulated to relax the glasses. The following procedure was used:

- heat the glass to 4000 K for 20 000 time steps,
- quench to a temperature of 293 K at a rate of 1×10^{14} K/s,
- relax the system at room temperature for 10 000 time steps

Although the pressure diminishes after quenching it could not be reduced to zero, as shown in Fig. 5. The selected quenching rate of 10^{14} K/s corresponds to the rate used for the initial glass fabrication.

These structures were used to compare the effects of irradiation with the effect of a pure volume change without irradiation.

3. Results

3.1. Effects of irradiation on the acoustic velocity

Fig. 6 shows the experimental results of the initial series of measurements by acoustic microscopy on R7T7 and CJ1 glass [20] externally irradiated by gold ions of multiple energy levels at various fluence values indicated in Table 1. The received irradiation dose increased in samples F1–F6 and was the same on both faces of each sample. The experimental procedure for irradiation and acoustic measurements has already been described [20] and is not repeated here, as the main focus of this article concerns the simulation results.

The measurements revealed a drop in the Rayleigh velocity as the irradiation dose increased (from sample F1–F6). Face 1 of CJ1 glass sample F6 was not irradiated, hence the outlying point in Fig. 6.

The longitudinal velocity was also measured in the material to determine Young's modulus, which diminished by 12% in R7T7 glass and 5% in CJ1 glass at the highest irradiation dose.

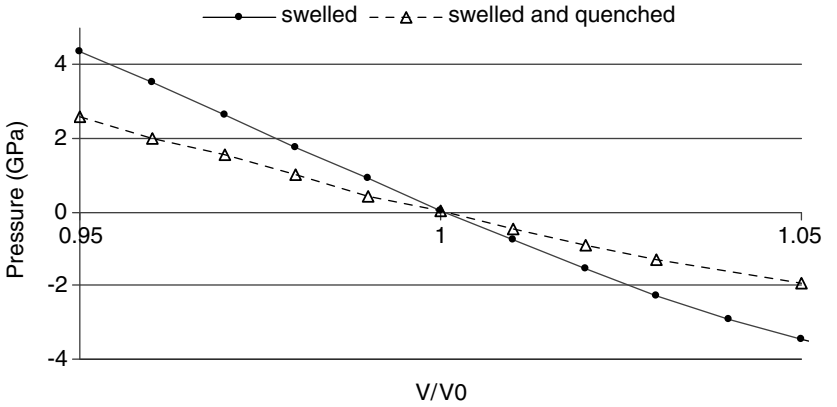

Fig. 5. Calculated pressure in the glass versus the artificial density variation (expressed as the ratio between the controlled volume and the initial volume). The pressure in the quenched glass (triangles) is lower than in the glass subjected only to an artificial density variation (dots).

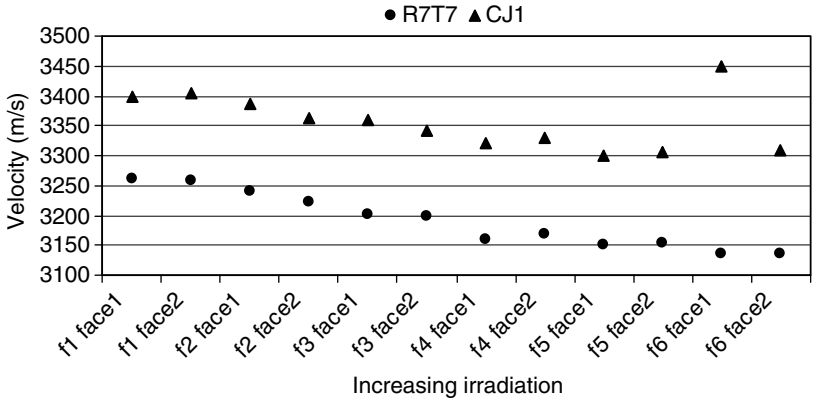

Fig. 6. Rayleigh velocities measured by acoustic microscopy in CJ1 and R7T7 glass.

Table 1
Irradiation level in glass specimens examined by acoustic microscopy

Energy (MeV)	Fluence (atoms/cm^2)					
	F1	F2	F3	F4	F5	F6
1	1.9×10^{15}	6.1×10^{15}	1.1×10^{16}	2.4×10^{16}	6.1×10^{16}	4.6×10^{17}
3.5	5.8×10^{15}	1.8×10^{16}	3.3×10^{16}	7.3×10^{16}	1.8×10^{17}	1.4×10^{18}
7	1.4×10^{16}	4.2×10^{16}	7.6×10^{16}	1.7×10^{17}	4.2×10^{17}	3.2×10^{18}
Total fluence	2.17×10^{16}	6.61×10^{16}	12×10^{16}	26.7×10^{16}	66.1×10^{16}	506×10^{16}

The external irradiation method employed here ensured uniform irradiation to a depth of about 2 μm below the surface, whereas the acoustic velocity measurement gives the values of Young's modulus corresponding to a probed depth of about 6 μm. The reduction in the acoustic velocity observed in the irradiated glass was therefore no doubt attenuated by the existence of an unirradiated zone along the wave path.

The acoustic velocity was measured by molecular dynamics in irradiated glasses previously subjected to up to 36 displacement cascades at an energy of 4 keV, corresponding to a total deposited energy of 2.19 eV/atom.

Fig. 7 shows a drop in the longitudinal and transverse velocities directly measured during the simulations, and Fig. 8 shows the drop in the Rayleigh velocity calculated from V_L and V_T using Eq. (2).

In the case of the molecular dynamics results, the uncertainty on the velocity measurements is about 2%, making it impossible to quantify the decrease with any precision. Moreover, the potentials used tend to increase the rigidity of the simulated glass structure; the resulting acoustic velocities are 30–40% higher than the values measured by ultrasound. Nevertheless, the V_L/V_T ratios between the simulated sodium borosilicate glass and the same glass studied experimentally are comparable (Table 2).

To be sure the algorithm used was not partly responsible for the shift in acoustic velocity, a pure silica glass was prepared with BKS potentials [21] for more precise structural and elastic characteristics. The V_L value obtained by MD is 6300 m/s, only 6% higher than the value of 5968 m/s reported in the literature [22].

The algorithm developed to measure the acoustic velocity can be considered valid, and was used qualitatively to account for the atomic origin of acoustic velocity variations in an irradiated sodium borosilicate glass specimen. As noted above, the potentials were too rigid, overestimating the simulated propagation velocities. Other reasons, such as the low temperature at which acoustic propagation was simulated (the experiments were carried out at room temperature) or the very short wave trains used for the simulation, can also account for some of the quantitative differences. The experimental method used sine wave packets at a frequency of about 500 MHz [23] whereas the numerical method described above uses comparatively much higher frequencies generating displacements of lower amplitude.

3.2. Effect of irradiation on the density

The atomic-scale changes in the glass were analyzed to understand the structural origin of the drop in the wave propagation velocities under irradiation. Experimental findings have demonstrated that the density of the French nuclear glass diminishes under irradiation. Results published by Peuget et al. [4] concerning curium-doped complex R7T7 glass specimens showed that the structure volume expansion increased with the irradiation dose. The volume change tends toward a saturation threshold according to an expression derived by Marples [24]

$$\frac{\Delta\rho}{\rho_0} = A(1 - e^{-\rho_0 VD}), \tag{6}$$

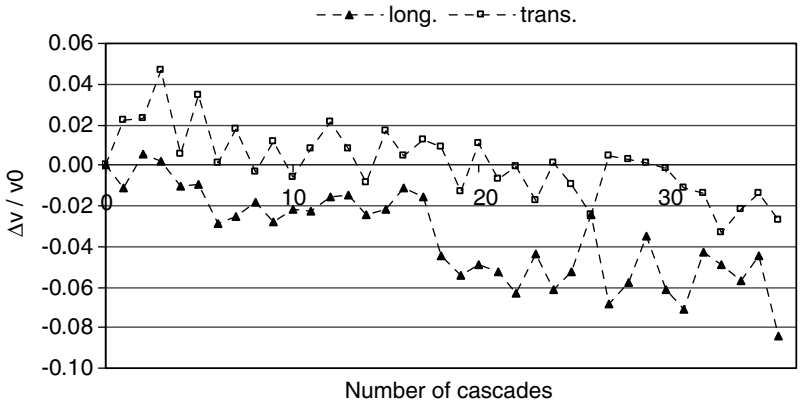

Fig. 7. Variation of longitudinal and transverse velocities in irradiated glass measured by molecular dynamics.

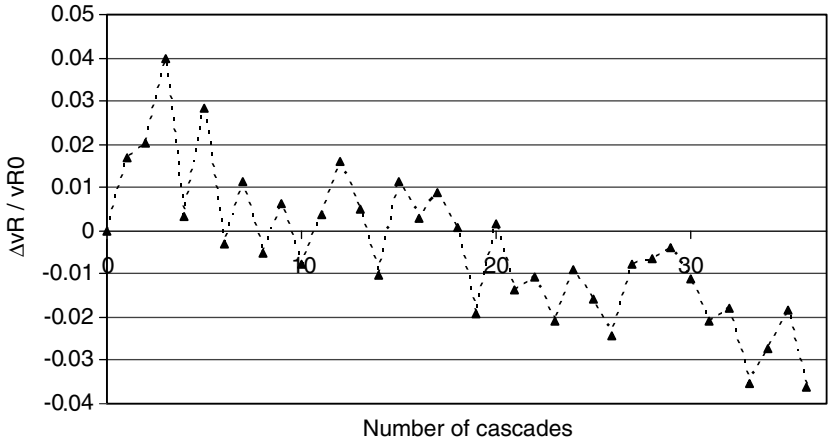

Fig. 8. Variation of Rayleigh velocities calculated from V_L and V_T values measured by molecular dynamics.

Table 2
Velocities (m/s) obtained by MD and by acoustic microscopy in CJ1 glass

	V_L	V_T	V_R	V_L/V_T
Results obtained by simulation				
Unirradiated glass	8493	4888	4499	1.737
After 36 cascades	8010	4780	4377	1.675
Results obtained by ultrasound				
Unirradiated glass	6100	3754	3419	1.625
Irradiated glass (maximum fluence)	5964	3623	3308	1.742

where ρ_0 is the glass density, A the maximum density variation (%), D the cumulative alpha decay (α/g) and V the glass volume damaged per alpha disintegration. $\Delta\rho$ corresponds to the density variation.

The simulation also revealed a reduction in the density of the CJ1 ternary glass after accumulating 36 displacement cascades. This density variation is plotted versus the deposited energy in Fig. 9.

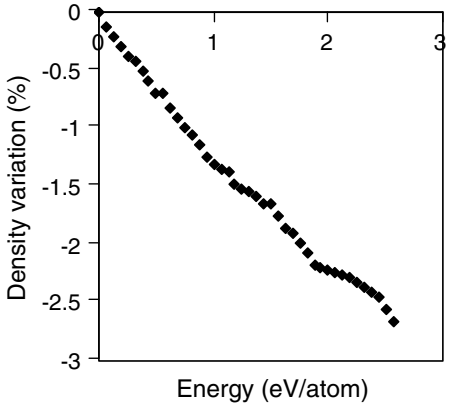

Fig. 9. Density variation versus deposited energy in CJ1 glass.

3.3. Effect of artificial volume changes on the acoustic velocity

In order to isolate the effect of pure volume change (without irradiation-specific structural damage) on the acoustic velocity, simulations were carried out on annealed and unannealed glass specimens artificially prepared with different densities. Calculations were performed for densities ranging from 5% compression to 10% expansion (Fig. 10(a)). This wide density range was necessary to identify an increasing trend for both the longitudinal and transverse velocities.

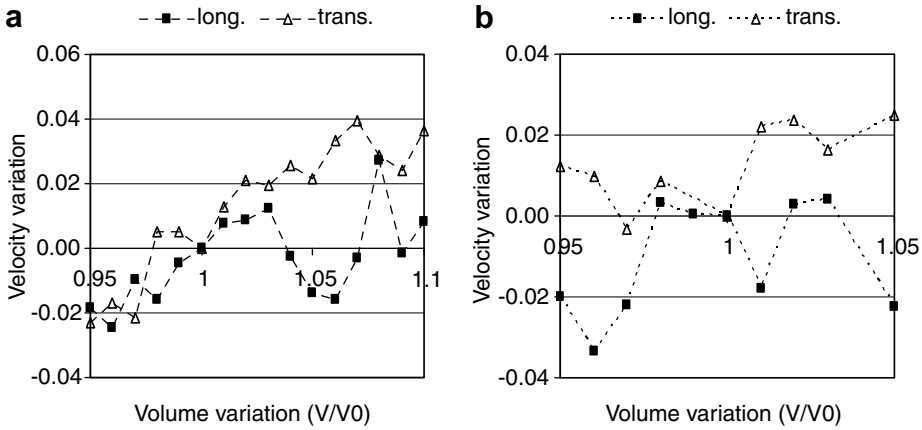

Fig. 10. Longitudinal and transverse velocity variations in glass after artificial expansion (a) then annealing (b).

The calculations are more difficult with glass after artificial expansion and annealing because the variations are of lower magnitude due to stress relief. In this case only a slight tendency toward increasing acoustic velocity was observed (Fig. 10(b)).

The observed effect was the opposite of that observed in irradiated glass. The acoustic velocity increases with swelling when the latter is induced artificially, but diminishes when the glass volume expansion is due to irradiation. This suggests a significant contribution from stresses induced in the glass by artificial swelling.

4. Structural analyses

Since the acoustic velocity increases with swelling in the artificially expanded glass and diminishes with swelling in the irradiated glass, atomic-scale structural differences should be detectable, as discussed in the following sections.

4.1. Effect on the boron coordination number

The variation in the number of boron atoms at coordination numbers 3 and 4 is plotted for artificially expanded (Fig. 11(a)) and annealed (Fig. 11(b)) glass and for irradiated glass (Fig. 12). The data for the artificially expanded glass concern structures compressed 5% and expanded 5%.

In each case, the conversion of BO_4 species to BO_3 is observed. The reduction in the quantity of BO_4 species in the irradiated glass was −9.1%, along with a 15% increase in the BO_3 species. The corresponding figures were −14.5% and +29%, respectively, for BO_4 and BO_3 in the case of 10% artificial volume variations (unannealed glass).

However, for an equivalent volume variation, the effect was greater in irradiated glass: a glass specimen artificially expanded by 3% (i.e. near the 2.3% expansion of the glass subjected to 36 displacement cascades) exhibited a reduction of −4.6% for BO_4 and an increase of +7.6% for BO_3, well below the variations observed under irradiation.

4.2. Effect on interatomic distances

An examination of the Si–O and Si–Si interatomic distances shows an increase of 1.16% and 3.39%, respectively, after an artificial volume increase of 10% in unannealed glass. The increase results in a shift of the first peak of the radial distribution functions (Fig. 13). A different type of shift was observed for B–O pairs (Fig. 14). The drop in the mean B coordination number has an effect, since the $^{[3]}$B–O distances are shorter than the $^{[4]}$B–O distances. The greater B–O distance induced by artificial swelling is partially offset by the larger number of BO_3 groups in place of BO_4 groups. Swenson et al. measured B–O distances of 1.47 Å for BO_4 species and 1.37 Å for BO_3 [25,26] species in borate glasses.

Examining the same radial distribution functions for irradiated glass shows broader first peaks as well as lower maximum values Fig. 15(a). In this case, the effect due to the conversion of BO_4 groups to BO_3 groups predominates in the B–O radial distribution function, which is shifted toward lower values, resulting in a reduction in the mean interatomic distance of the B–O pairs from 1.478 Å to 1.474 Å (Fig. 15(b)).

4.3. Effect on angular distributions

Fig. 16 shows the change in the F–O–F angular distribution (where F = Si or B) in artificially expanded glass. The shift in the angular distribution toward increasing angles was confirmed by calculating the mean values: the Si–O–Si, Si–O–B and B–O–B angles increase by +1.73%, +2.56%, and +5.04%, respectively, for a 10% artificial volume variation.

The O–Si–O angles do not exhibit significant variations, whereas the O–B–O angles show a broader distribution around the mean value. It is again interesting to highlight the influence of the conversion of BO_4 groups to BO_3: the mean angle of the O–B_4–O triplets is 109° compared with 120° for the O–B_3–O triplets, hence an asymmetric distribution variation as shown in Fig. 17. The shoulder

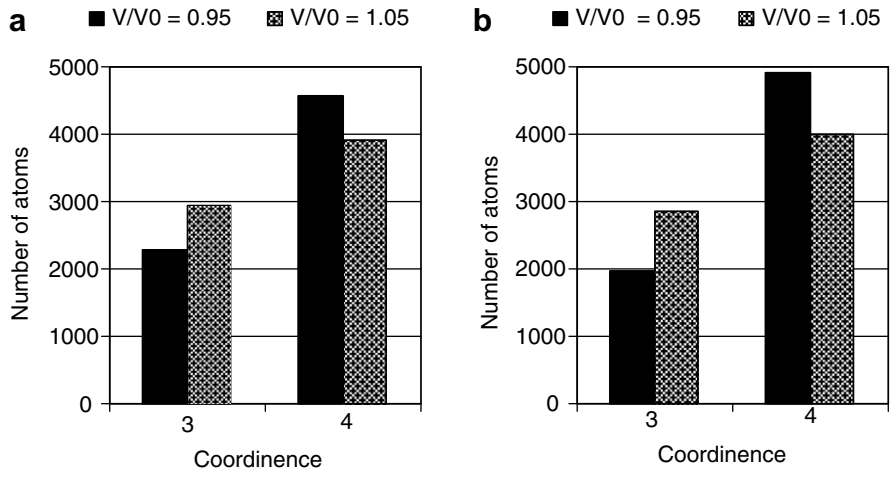

Fig. 11. Boron coordination number in glass artificially expanded (a) then annealed (b).

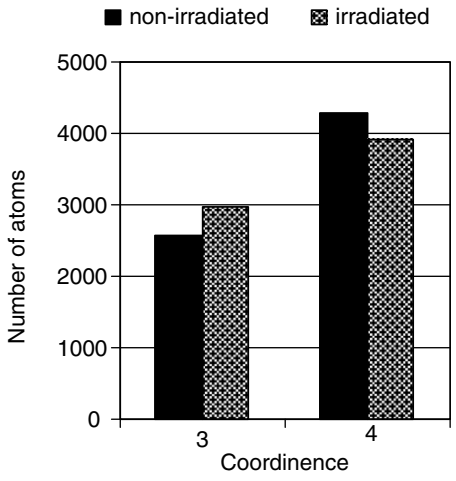

Fig. 12. Boron coordination number in irradiated glass.

that appears near 120° is directly correlated with the increased concentration of O–B_3–O triplets.

In the irradiated glass, the variation in the angles between the two network formers and oxygen is less significant, but still visible. Fig. 18 illustrates the trend toward diminishing Si–O–Si angles. The mean Si–O–Si and Si–O–B angles vary by −0.73% and −0.35%, respectively.

This behavior is typical of a broader distribution for O–Si–O triplets (Fig. 19) with a lower peak and broader base. The influence of the conversion of BO_4 groups to BO_3 on the O–B–O angles is greater here than on the extended distribution, and results in an overall shift in the distribution toward increasing angles (Fig. 20).

4.4. Effect on rings

We supplemented this study of structural changes by examining the ring size distributions and ring compositions. We counted the rings in the structure as in previous work [5] using the following method: for each oxygen atom we determined the smallest ring containing that atom. The resulting set of rings provides an overview of the ring distribution in the glass structure.

We first determined the mean composition of the rings depending on their size (Fig. 21) by discriminating between

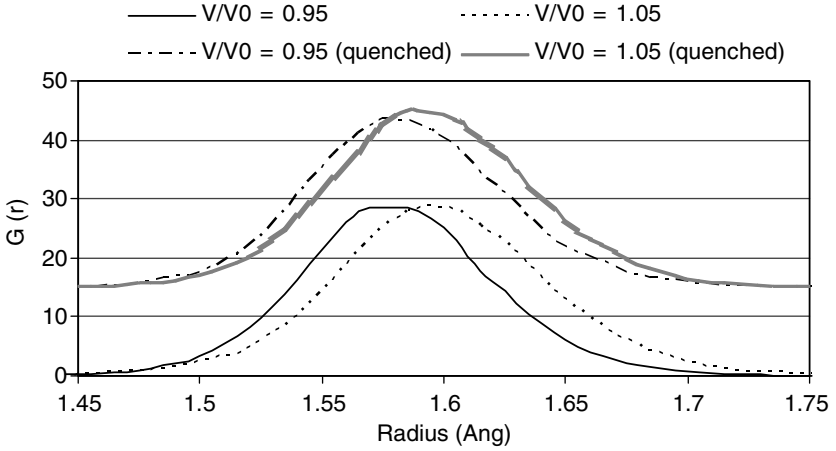

Fig. 13. First peak of the radial distribution function of Si–O pairs (artificially expanded glass); the curves for the annealed glass are shifted.

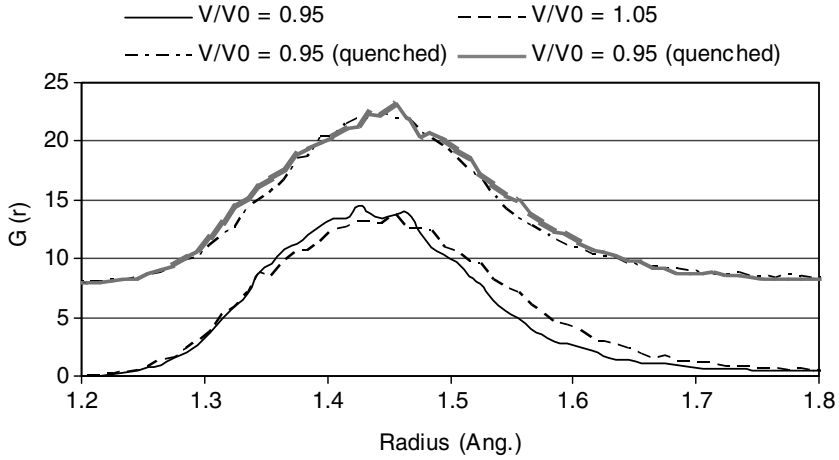

Fig. 14. First peak of the radial distribution function of B–O pairs (artificially expanded glass); the curves for the annealed glass are shifted.

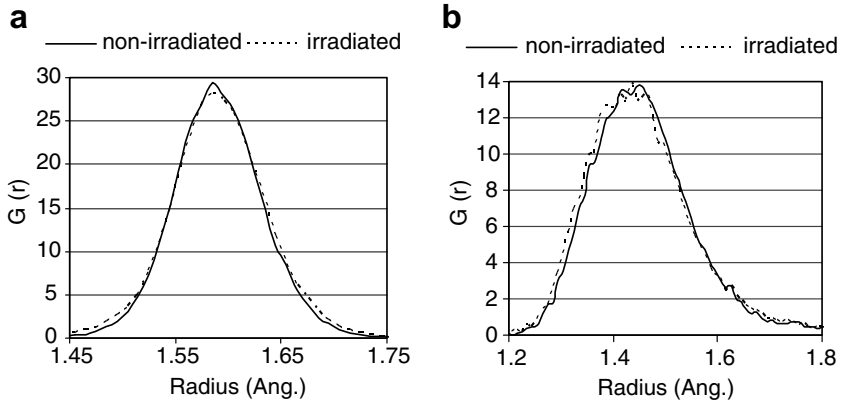

Fig. 15. First peak of the radial distribution function in irradiated glass for Si–O pairs (a) and B–O pairs (b).

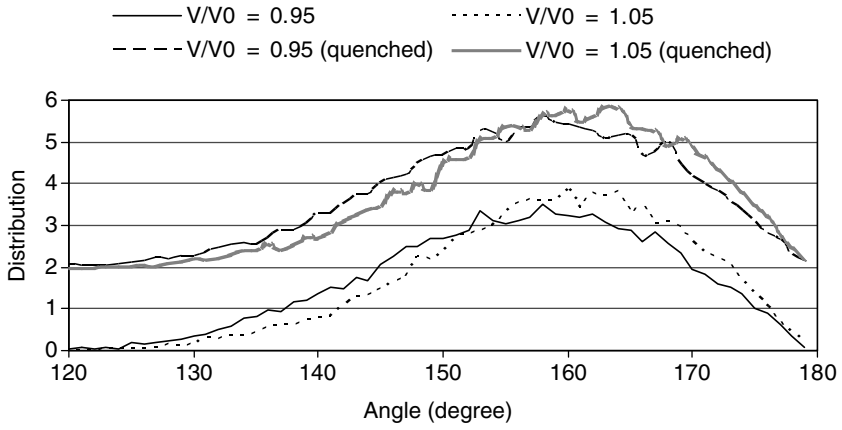

Fig. 16. Angular distribution of Si–O–Si triplets (artificially expanded glass).

boron at coordination numbers 3 and 4, and oxygen at coordination numbers 2 and 3.

The results in pristine glass were as follows:

- 2-member rings (which exist because of the relatively high quenching speed used to fabricate the glass) virtually all comprise 4-coordinate boron and 3-coordinate oxygen;
- the proportion of tricoordinate oxygen diminishes very quickly with the ring size, and is nil for ring sizes exceeding 5;
- the proportion of 3-coordinate boron increases with the ring size, while the 4-coordinate boron fraction diminishes.

A detailed description of variations in the number of rings versus their size reveals an increase in large rings

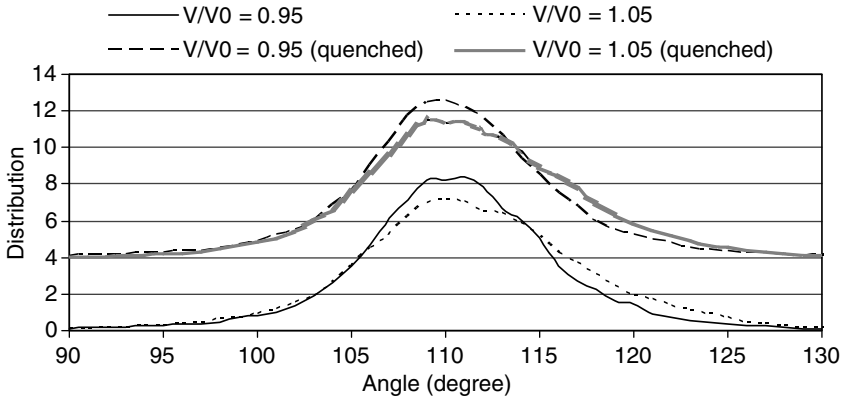

Fig. 17. Angular distribution of O–B–O triplets (artificially expanded glass).

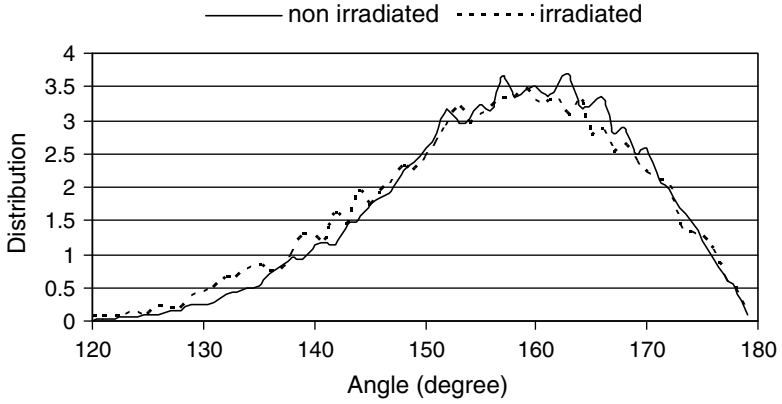

Fig. 18. Angular distribution of Si–O–Si triplets (irradiated glass).

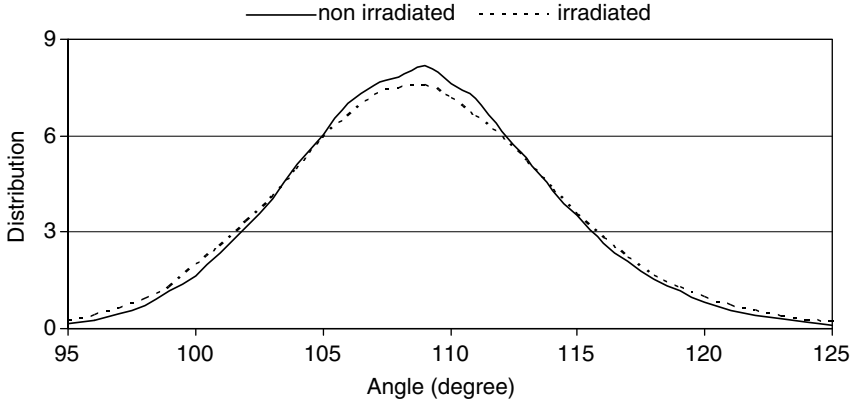

Fig. 19. Angular distribution of O–Si–O triplets (irradiated glass).

(exceeding 5 members) and a reduction in small ones (fewer than 5 members) in the case of an artificial volume increase (Fig. 22(a)) and annealing (Fig. 22(b)). The mean size for a 10% total volume expansion increased from 4.857 to 4.964. The reduction in the number of small rings is correlated with the drop in tricoordinate oxygen (Fig. 23), while the increase in the number of large rings is correlated with the previously mentioned rise in the number of tricoordinate boron and nonbridging oxygens. These observations are consistent with previous findings showing an overall shift in the distributions towards increasing values both for the radial distribution functions and the angular distributions.

The ring size distribution increases in the irradiated glass (Fig. 24), resulting in a larger number of rings with 4 or fewer members or with more than 6 members, and a smaller number of intermediate rings (5 or 6 members). Although the reduction in the boron coordination number, and the increasing number of nonbridging oxygens (Fig. 25) accounts

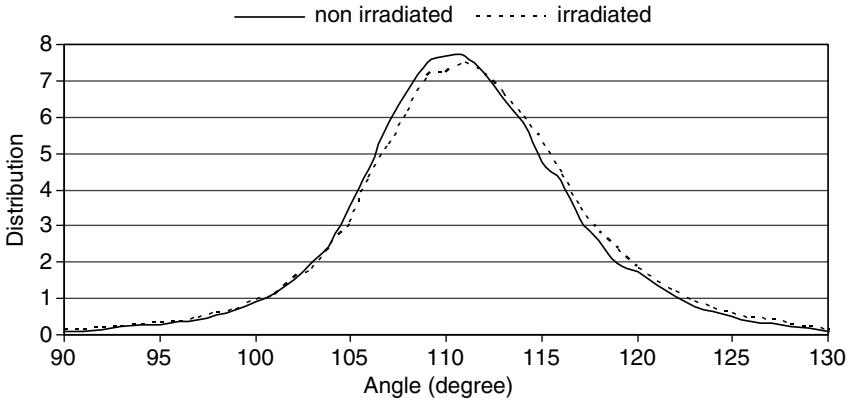

Fig. 20. Angular distribution of O–B–O triplets (irradiated glass).

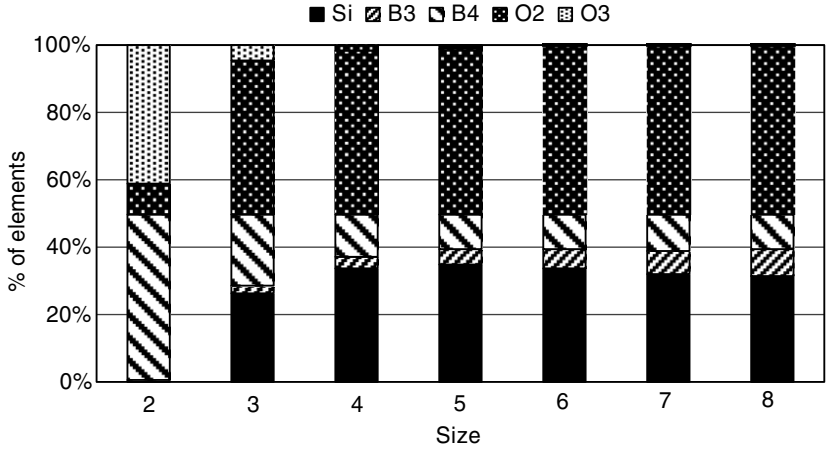

Fig. 21. Mean composition versus ring size (in pristine CJ1 glass).

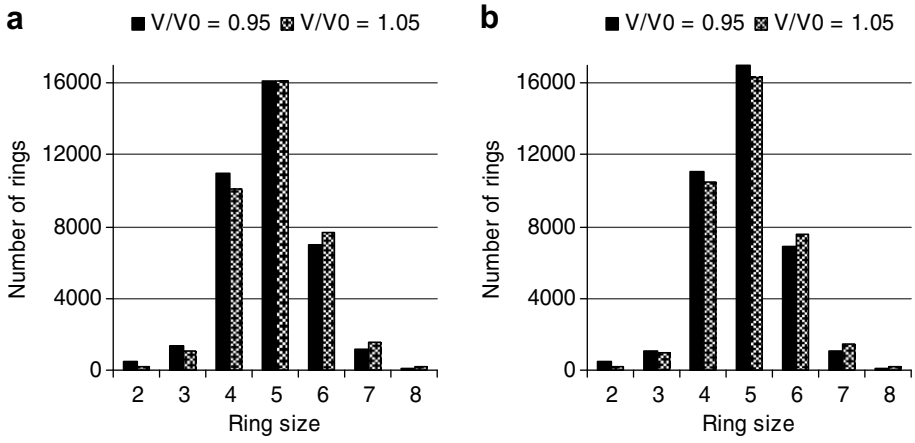

Fig. 22. Ring distribution in glass artificially expanded (a) then annealed (b).

for the higher number of large rings, the structural data capable of accounting for the increasing number of small rings are not clear.

This phenomenon may be due to quenching, as the irradiated glass passes through a high-temperature phase followed by quenching at a higher rate than initially. A similar extension of the ring size distribution was observed in CJ1 glass by Bureau et al. [27] who investigated the effects of the quenching rate on the glass structures. The number of smaller and larger rings was observed to increase, and the concentration of intermediate ring sizes diminished as the glass quenching rate [27] increased.

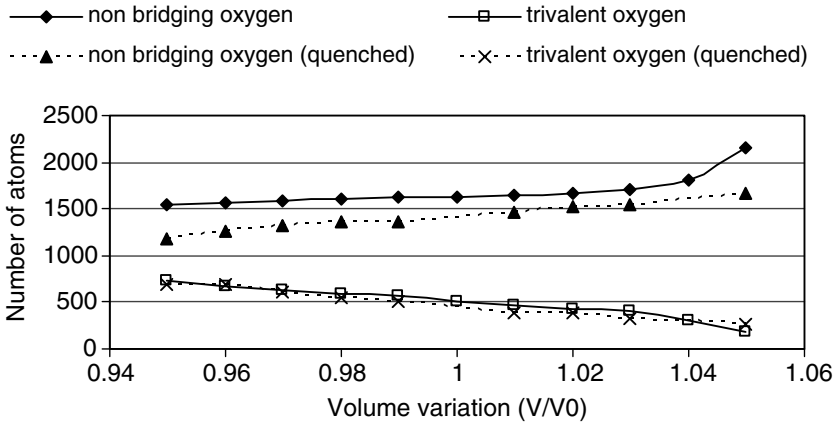

Fig. 23. Variation in the number of nonbridging and tricoordinate oxygens in glass artificially expanded (solid line) then annealed (broken line).

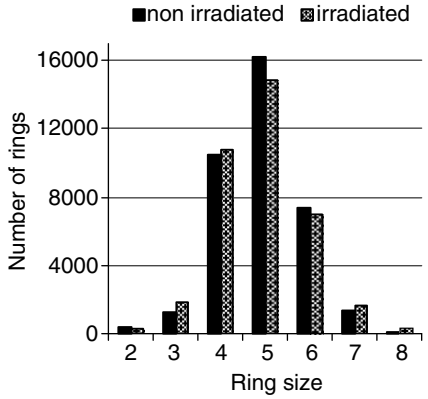

Fig. 24. Ring size distribution in irradiated glass.

5. Discussion

Volume expansion results in different structural changes depending on its origin. The behavior of an artificially expanded glass structure is characterized by a shift in the distributions toward higher values. This was observed for the angular distributions, the radial distribution functions and the ring size distributions. Several features attributable mainly to the conversion of BO_4 species to BO_3, were noted: The shift in the angular distribution for O–B–O is asymmetric because of the difference in the mean angle between O–B_4–O and O–B_3–O; similarly, the B–O radial distribution function is affected by the difference in the interatomic distance between B_4–O and B_3–O pairs.

Artificial swelling of the glass structure induces stresses that increase the acoustic velocity. It is generally acknowledged that the acoustic velocity diminishes as the material density diminishes [28]. The opposite is observed here, suggesting that the stress loading in the glass structure has a decisive role in increasing the acoustic wave propagation velocity; a secondary effect of the stress loading is the overall shift in the distributions toward higher values, as noted above.

Completely different phenomena are observed in irradiated glass: the distributions are systematically broader. With few exceptions related to the declining boron coordination number, the angular distributions, radial distribution functions and ring-size distributions are characterized by lower peak values and a broader range. This general behavior resembles an increasingly disordered structure.

Once again, the conversion of BO_4 to BO_3 occurs with the same consequences on the O–B–O angular distributions

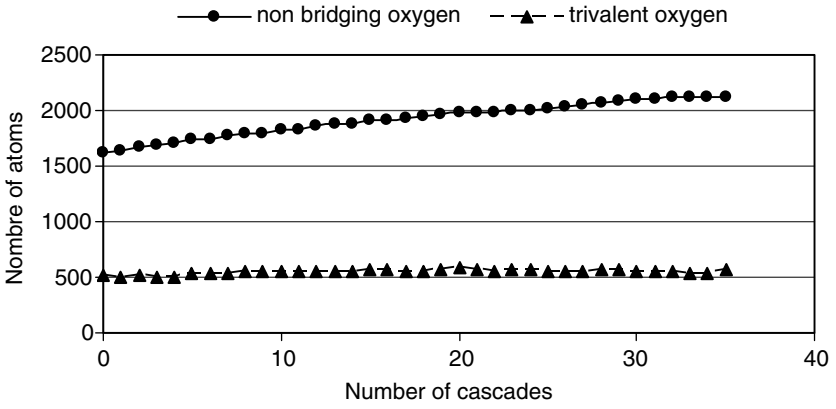

Fig. 25. Variation in the number of nonbridging and tricoordinate oxygens in irradiated glass.

or the B–O distances for artificially expanded glass. Irradiation by ballistic collisions thus increases the lattice disorder that is responsible for the decrease in acoustic velocity.

Let us reconsider the notion of local quenching induced by the passage of projectiles. The temperatures reached during a cascade are difficult to determine; the agitation of the atoms does not correspond to equilibrated thermal agitation but rather to a temporary state away from equilibrium, and the agitation is very heterogeneous in the cascade core region. Nevertheless, zone-by-zone measurements of atomic velocities [27] led to estimated temperatures of about 10 000 K along the projectile path over time periods so short that an equilibrium liquid state could probably not be reached.

Fig. 26 shows the estimated quenching rates versus time in a glass volume of about a hundred atoms at the heart of a 4 keV displacement cascade. The temperature drops at quenching rates between 10^{16} and 10^{14} K/s. The analogy between the consequences of a displacement cascade (which will heat and then rapidly quench a region of the glass) and the effects of a modified quenching rate during glass fabrication is thus not unfounded.

We will not detail the effects of quenching, which have already been largely discussed by Bureau et al. [27] for CJ1 glass in studies of glass specimens prepared at different quenching rates. The observed Si–O interatomic distances and ring-size distributions show that the distributions became broader as the quenching rates increased. An increase in the number of small rings in rapidly quenched glass had already been observed by Ito et al. [29,30] in Na_2O–MgO–CaO–Al_2O_3–SiO_2 glass, but the distribution of larger rings was not reported.

Increasing the quenching rates thus produces effects comparable to those of irradiation, suggesting that at least some of the structural effects within a displacement cascade and their consequences on the acoustic velocity are due to a modification of the quenching rate.

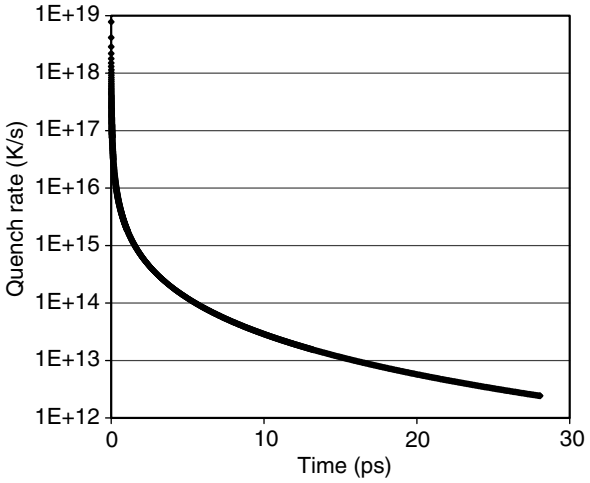

Fig. 26. Estimated quenching rate in a zone along the projectile path.

We supplemented this study by molecular dynamics measurements of the acoustic velocity in glass specimens prepared at different quenching rates. First, a ternary CJ1 glass structure with 64 000 atoms was prepared with a quenching rate of 5×10^{12} K/s (whereas the previously investigated structures had been prepared at 10^{14} K/s). The rise in the acoustic wave propagation velocities was about 3% (longitudinal) and 4% (transverse) in the glass quenched at 5×10^{12} K/s compared with the glass quenched at 10^{14} K/s.

A similar study, only the results of which are reported here, was carried out on glass specimens of a different chemical composition (molar percentages: 63.77% SiO_2, 13.39% Na_2O, 16.98% B_2O_3, 4.05% Al_2O_3, 1.81% ZrO_2) prepared by molecular dynamics with quenching rates between 5×10^{12} K/s and 10^{16} K/s. Once again, the longitudinal and transverse acoustic velocities diminished as the quenching rates increased – mainly between 5×10^{12} K/s and 10^{14} K/s.

The drop in the acoustic velocity following ballistic collisions in the glass is similar in many respects to the drop in the same velocity in glass prepared with higher quenching rates.

6. Conclusion

The development of a molecular dynamics method simulating the propagation of acoustic waves allowed their propagation velocities to be measured in borosilicate glasses. The qualitative results obtained in glass irradiated by heavy ions correctly reproduces the experimental results, i.e. a reduction in the acoustic wave propagation velocity in irradiated glass.

These changes in the mechanical properties were correlated with structural changes, in particular increased disorder in the glass. The greater disorder results in broadening of the characteristic distributions of the glass: distances, angles, and ring sizes.

Similarities were clearly observed between the effects of irradiation and the effects of higher quenching rates on the acoustic wave propagation velocities.

An additional study of glass artificially expanded by homothetic volume transformation shows that a reduction in acoustic velocity is not necessarily associated with swelling. The artificial volume change combined with increased stresses in the glass results in higher acoustic velocities.

References

[1] W.J. Weber, R.C. Ewing, C.A. Angell, G.W. Arnold, A.N. Cormack, J.-M. Delaye, D.L. Griscom, L.W. Hobbs, A. Navrotsky, D.L. Price, A.M. Stoneham, M.C. Weinberg, J. Mater. Res. 12 (1997) 1946.
[2] Y. Inagaki, H. Furuya, Y. Ono, K. Idemitsu, T. Banba, S. Matsumoto, S. Muraoka, Mater. Res. Soc. Sympos. Proceed. 294 (1993) 191.
[3] S. Peuget, P.Y. Noël, J.L. Loubet, S. Pavan, P. Nivet, A. Chenet, Nucl. Instrum. Meth. Phys. Res. 246 (2006) 379.
[4] S. Peuget, J.-N. Cachia, C. Jégou, X. Deschanels, D. Roudil, V. Broudic, J.-M. Delaye, J.-M. Bart, J. Nucl. Mater. 354 (2006) 1.

[5] J.-M. Delaye, D. Ghaleb, Phys. Rev. B 61 (2000) 14481.
[6] J.-M. Delaye, D. Ghaleb, Nucl. Instrum. Meth. B 191 (2002) 10.
[7] G.J. Martyna, M.E. Tuckerman, D.J. Tobias, M.L. Klein, Mol. Phys. 87 (1996) 1117.
[8] Hj. Matzke, E. Vernaz, J. Nucl. Mater. 201 (1993) 295.
[9] S. Peuget, J.-M. Delaye, D. Ghaleb, X. Deschanels, Technical Note DTCD/SECM/2005/15, CEA Internal Document, 2005.
[10] C. Jegou, PhD thesis, University of Montpellier II, 1998.
[11] I.A. Viktorov, Rayleigh and Lamb Waves, Plenum, New York, 1967.
[12] L. Mesguich, J.M. Saurel, University of Montpellier II, Private communication.
[13] J.-M. Delaye, L. Cormier, D. Ghaleb, G. Calas, J. Non-Cryst. Solids 293–295 (2001) 290.
[14] L. Cormier, D. Ghaleb, J.-M. Delaye, G. Calas, Phys. Rev. B 61 (2000) 14495.
[15] S.W. De Leeuw, J.W. Perram, E.R. Smith, Proc. Roy. Soc. Lond. A 373 (1980) 27.
[16] F.H. Stillinger, T.A. Weber, Phys. Rev. B 31 (1985) 5262.
[17] B.P. Feuston, S.H. Garofalini, J. Chem. Phys. 89 (1988) 5818.
[18] J.F. Ziegler, J.P. Biersack, U. Littmark, The Stopping and Range of Ions in Matter, Pergamon, New York, 1985.
[19] J.-M. Delaye, D. Ghaleb, Phys. Rev. B 71 (2005) 224203.
[20] F. Augereau, G. Despaux, S. Peuget, J. Nucl. Mater., submitted for publication.
[21] B.W.H. Van Beest, G.J. Kramer, R.A. Van Santen, Phys. Rev. Lett. 64 (1990) 1955.
[22] D.R. Lide, Handbook of Chemistry and Physics, 79th ed., 1998–1999, p. 14.
[23] F. Augereau, Personal communication Caractérisation microacoustique de verres irradiés par implantation ionique, LAIN/UM2, 2005.
[24] J.A.C. Marples, Nucl. Instrum. Meth. B 32 (1988) 480.
[25] J. Swenson, L. Börjesson, W.S. Howells, Phys. Rev. B 52 (1995) 9310.
[26] H. Doweidar, M.S. El-Shahawi, F.M. Reicha, H.A. Silim, K. El-Egaly, J. Phys. D: Appl. Phys. 23 (1990) 1441.
[27] G. Bureau, J.-M. Delaye, S. Peuget, G. Calas, N. Deladerrière, Proceedings of the Materiaux 2006, Dijon, France, 13–17 November, 2006.
[28] E. Rat, M. Foret, G. Massiera, R. Vialla, M. Arai, R. Vacher, E. Courtens, Phys. Rev. B 72 (2005) 214204.
[29] S. Ito, T. Taniguchi, J. Non-Cryst. Solids 349 (2004) 173.
[30] T. Taniguchi, S. Ito, Proceedings of the XIX International Congress on Glass, Edinburgh, 1–6 July 2001, Phys. Chem. Glass. 43C (2001) 493.